Journal of the Australian Ceramic Society (2019) 55:729–736
https://doi.org/10.1007/s41779-018-0284-2

RESEARCH

High-energy ball milling of lead-free piezoceramic: influence of milling medium on properties

Bhupender Rawal[1] · Prashant Dixit[1] · B. Praveenkumar[1] · H. S. Panda[2]

Received: 13 April 2018 / Revised: 7 September 2018 / Accepted: 2 November 2018 / Published online: 8 November 2018

Abstract

The study highlights the effect of high-energy ball milling (HEBM) in dry and wet mode, in comparison to conventional ball milling (CBM), on NKN-based lead-free piezoceramics. The particle size reduced significantly from 1.97 μm (CBM) to 115 nm after wet HEBM which enhanced the piezoelectric property significantly. HEBM influenced the microstructure of the samples which improved the density, and the samples exhibited excellent ferroelectric character, stable ageing and electrical fatigue behaviour. As compared to CBM, dielectric constant increased nearly 50%, while piezoelectric charge coefficient (d_{33}) increased more than double by wet HEBM. The wet HEBM samples also showed better ferroelectric properties and higher Curie temperature (~ 320 °C) along with improved resistance to thermal annealing due to stable ferroelectric polarisation state.

Keywords High-energy ball milling · Lead-free · Ageing · Thermal stability · Fatigue

Introduction

Environment friendly lead-free piezoelectric ceramics have been gaining interest as an alternative to the lead-based piezoceramics which are widely used as actuator, transducer and sensor [1]. Alkaline niobate–based material, in the recent years, has shown very promising behaviour and is a strong contender to PZT-based perovskites because of reasonably high Curie temperature (T_C) and good piezoelectric properties [2–4]. NKN-based lead-free compositions have been explored extensively by researchers, and Li-Ta–doped NKN is one of the most investigated ones among these [5–11]. Li-Ta–doped NKN has been synthesised using many routes, such as solid-state reaction [5, 6], hydrothermal [12], sol-gel [13] and solvothermal [14]. The ultimate properties of the piezoceramics depend a lot on the powder morphology. Chemical routes are an effective way to prepare nanoparticles, but the process demands high-purity reactants which are quiet expensive. The high-energy ball milling (HEBM) is considered as an effective and economical way to modify the morphology for producing fine powders. The HEBM has been successfully utilised for mechanochemical synthesis, preparing activated powders, modifying calcination temperature, mechanical alloying and reducing the particle size of a variety of materials such as PZT-based piezoceramics [15–17], PMN-PT [18, 19], silicon nitride [20], BZT [21], barium ferrites [22], lead titanate powders [23], NKN-based ceramics [24–26], alumina [27] and Bi-based lead-free ceramics [28, 29].

It has been observed that the properties of the powders vary widely depending upon the ball milling conditions. NKN-based ceramics have been synthesised and/or modified using HEBM. Van [30, 31], in 2013, claimed to have directly synthesised the NKN powder for the first time using a mechanochemical method and studied the effects of the ball-to-powder mass ratio and milling speed on the synthesis of $(K_{0.5}Na_{0.5})NbO_3$ nanopowders by a reactive high-energy dry ball milling method. The HEBM-modified NKN powder has been reported to have better properties than conventionally prepared NKN [24]. The HEBM has been used in experiments either in wet mode or in dry mode [25, 26, 31]. Liu et al. [32] derived $(Na_{0.5}K_{0.5})NbO_3$ nanocrystalline powder by high-energy dry ball milling, followed by

✉ Bhupender Rawal
bsrawal@arde.drdo.in

Prashant Dixit
contactprashant.adm@gmail.com

B. Praveenkumar
Praveenkumar@arde.drdo.in

H. S. Panda
Himanshusp@diat.ac.in

[1] Armament Research and Development Establishment, Pune 411021, India

[2] Defence Institute of Advanced Technology, Pune 411025, India

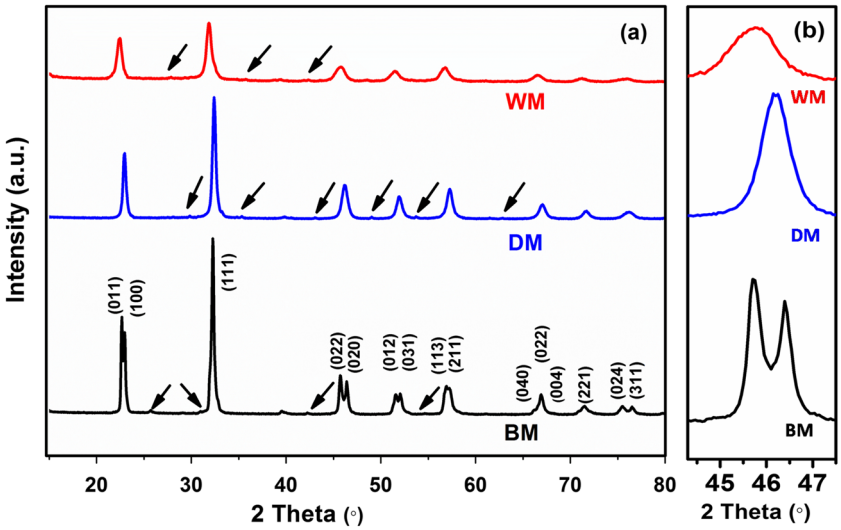

Fig. 1 **a**, **b** X-ray diffraction pattern of NKLNT ceramic powder described as BM, DM and WM synthesised using different milling conditions. Note: Arrows denote secondary phase

calcination. Wet HEBM has been reported to improve the sinterability of lead-free $Na_{0.5}K_{0.5}NbO_3$ piezoelectric ceramics [33]. For PZT-based compositions also, superior piezoelectric and dielectric properties have been reported in the HEBM samples as compared to the conventional ball milling (CBM) [15]. BenAbdeslam et al. [34] showed that the calcium phosphates give different results under wet and dry milling. However, specific studies focusing on the effect of high-energy ball milling in wet mode and dry mode for Li-Ta–doped NKN-based ceramics are missing.

Better dielectric and piezoelectric properties in piezoceramics are no doubt advantageous and are a point of focus of most of the studies. But, when it comes to application, certain other aspects like thermal stability, electrical fatigue

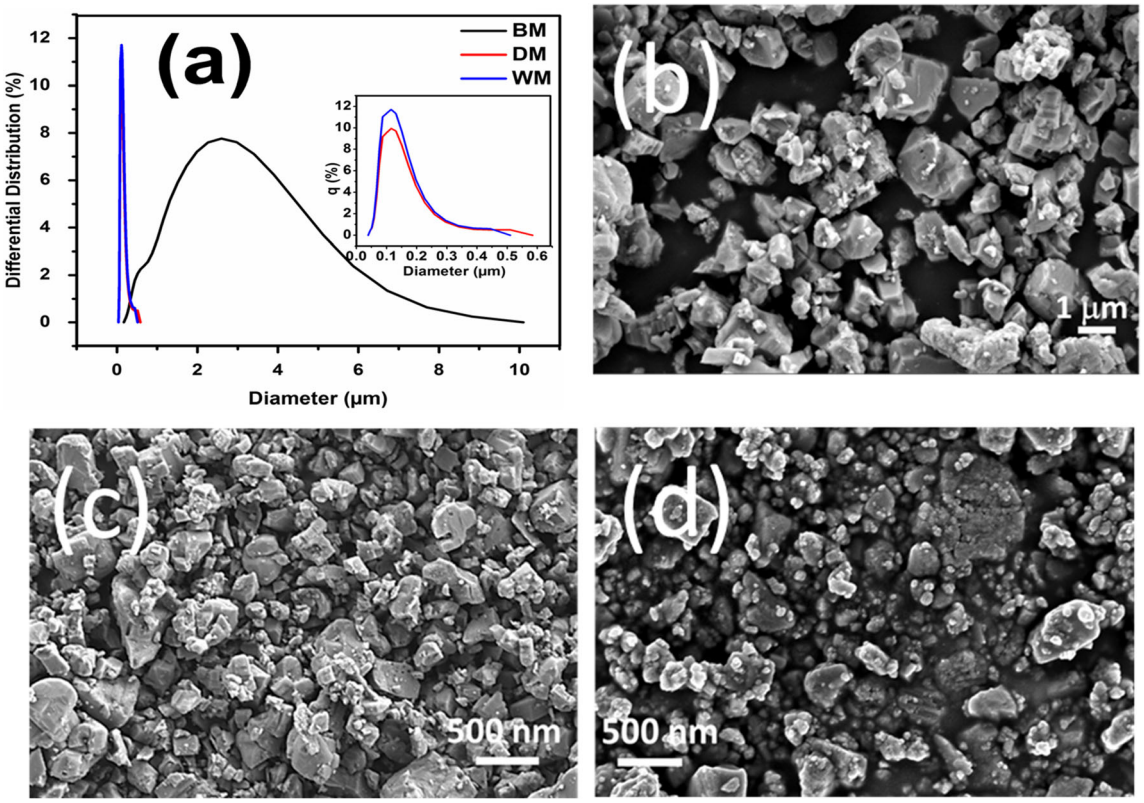

Fig. 2 **a** Particle size distribution of the powders synthesised by different milling conditions and SEM of **b** conventional ball milled (BM), **c** 10-h dry HEBM (DM) and **d** 10-h wet HEBM (WM) NKLNT ceramic powder

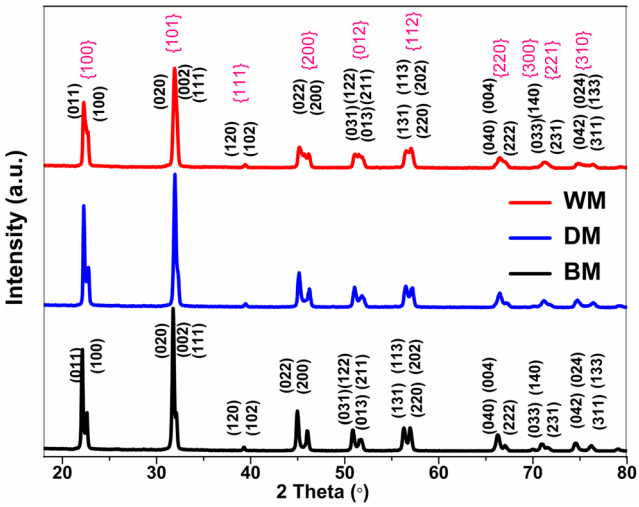

Fig. 3 XRD patterns of the conventional ball–milled (BM), high-energy dry–milled (DM) and high-energy wet–milled (WM) NKLNT ceramics sintered at 1120 °C for 2 h (indexing for monoclinic, e.g. in red colour)

and ageing behaviour are equally important parameters which are overlooked by researchers and seldom reported. Very few studies are available which gives an insight into ageing, fatigue and thermal stability behaviour of NKN-based lead-free piezoceramics [9, 35–37].

In this paper, a comparative study of the dry and wet HEBM with CBM has been reported. Li-Ta–doped NKN composition, $0.95(Na_{0.52}K_{0.48})NbO_3$–$0.05LiTaO_3$, has been selected for the study, with a special emphasis given on the stability of piezoelectric and ferroelectric properties along with dielectric and microstructural studies.

Materials and methods

In this work, lead-free composition $0.95(Na_{0.52}K_{0.48})NbO_3$–$0.05LiTaO_3$, henceforth abbreviated as NKLNT, was prepared by a conventional solid-state method using sodium carbonate (Na_2CO_3), potassium carbonate (K_2CO_3), niobium pentoxide (Nb_2O_5), lithium carbonate (Li_2CO_3) and tantalum pentoxide (Ta_2O_5) (all Sigma-Aldrich, purity of 99% or more) as raw materials. The raw materials were dried right before use at 220 °C for 90 min because of their hygroscopic nature and weighed in appropriate proportions according to the stoichiometry formula. They were homogeneously mixed in high-density polyethylene (HDPE) jar for 24 h using zirconia balls in ethanol medium by roller jar-type conventional ball mill. The mixture was dried and calcined at 860 °C for 5 h and remilled in the ethanol medium for 24 h in CBM. This powder was divided into three parts. The first part was further ball milled for 10 h and was labelled as BM (ball milled). The second part was high-energy ball milled without any solvent, using a planetary ball mill (Retsch PM 100) at 300 RPM with tungsten carbide balls for 10 h, which was labelled as DM (dry milled). Similarly, the third part was high-energy ball milled using 60% by wt. of distilled water as solvent, keeping other parameters constant, and labelled as WM (wet milled).

The particle size of the powders was examined using a laser particle size analyser (Horiba LA-960). The milled and dried powders were granulated by adding polyvinyl alcohol as binder and uniaxially pressed into circular pellets of 17 mm diameter and 2 mm thickness. After burning off the binder, the pellets were sintered in a covered alumina crucible at 1120 °C for 2 h. The sintered pellets were lapped to a thickness of 1.5 mm, and the bulk density of the sintered compacts was obtained by the Archimedes method. X-ray diffractometer (Bruker AXS D8 Advance) was used over a 2θ range from 15 to 80° to determine the crystal structures of the as-milled powder and sintered samples. TOPAS 4.2 software was employed for carrying out the Rietveld analysis of the XRD data. The microstructures of the powders and the fractured surfaces of the samples were studied using field emission scanning electron microscopy (FESEM) (Merlin, Carl Zeiss), and the Quantimet software was utilised to ascertain the average particle and grain size of the powders and sintered samples.

For electrical measurements, silver paste was applied on both sides of the sintered samples as electrodes and fired at 650 °C for 1 h before poling under a DC field of 2 kV mm^{-1} at 100 °C for 45 min in the silicon oil bath. The temperature dependence of dielectric properties was measured at 1 kHz using a broadband dielectric spectrometer (Novocontrol). The piezoelectric charge coefficient (d_{33}), capacitance (C) and loss factor (tan δ) were measured with a d_{33} meter (Piezotest PM300). The poled samples were heated at a specified temperature for 10 min before determining the d_{33} to study the thermal stability. The ageing

Table 1 Rietveld refinement results for the BM, DM and WM samples

Sample	Phase	R_{wp}	GOF	Cell vol. (Å)^3	Cry. density (g cm^{-3})	a	b	c
BM	Ortho (*Amm2*)	7.04	3.13	126.08	4.605	4.03686	5.58934	5.58763
DM	Ortho (*Amm2*)	8.66	3.77	126.07	4.6054	4.03852	5.58751	5.58696
WM		8.38	3.81					
79.4 vol.%	Ortho (*Amm2*)	–	–	126.326	4.5961	4.02970	5.5848	5.6132
20.6 vol.%	Mono (*Pm*)	$\beta = 90.2244$		62.936	4.613	3.94047	4.00870	3.98425

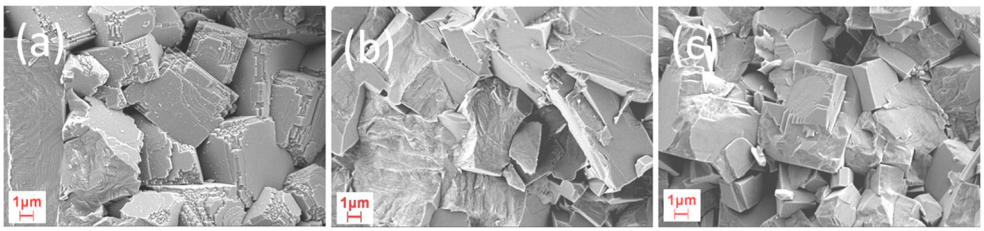

Fig. 4 FESEM of a fractured surface of the **a** BM, **b** DM and **c** WM samples sintered at the 1120 °C for 2 h

rate was calculated by measuring the d_{33} at desired time after poling. aixACCT TF Analyzer 2000 was utilised to ascertain the ferroelectric properties and electrical fatigue of the samples under cyclic electrical loading.

Results and discussion

Figure 1a, b illustrates the X-ray diffraction patterns of as-milled NKLNT-BM, NKLNT-DM and NKLNT-WM ceramic powders and confirms the formation of perovskite-structured NKLNT. However, the presence of secondary phase could also be observed, which has been marked with black arrows and identified as tungsten bronze-structured $K_3Li_2Nb_5O_{15}$ [38]. After HEBM, significant broadening and decrease in the peak intensity of the diffraction peaks can be seen which indicates the reduction in the crystallite size [39].

The particle size distribution of the NKLNT powders after various milling conditions is shown in Fig. 2a. The considerable reduction in particle size is observed by using the HEBM. The initial mean particle size (d_{50}) of BM powder is around 1.97 μm, which significantly reduced to a d_{50} of 130 nm and 115 nm after 10 h of dry and wet HEBM, respectively. Figure 2b–d shows FESEM micrographs of the BM, DM and WM powders, respectively. The BM sample has particles of an average diameter of 2.1 μm. Some very fine particles of 0.3–0.6 μm size are also interspersed. The HEBM samples also display a bimodal distribution of particles. The approximate average size of fine particles is ~100 nm and ~65 nm while the average size of coarse particles is ~420 nm and ~

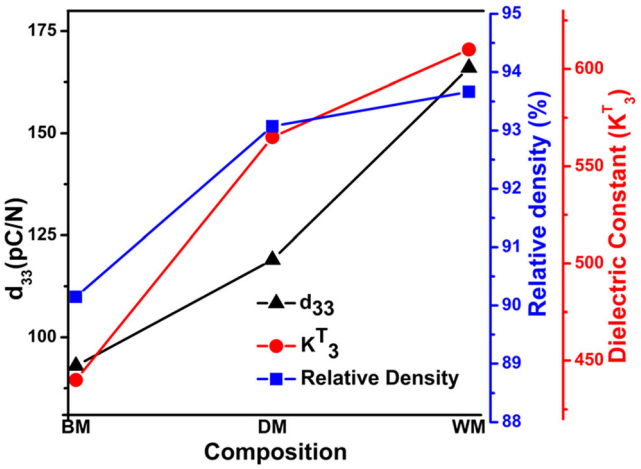

Fig. 5 Piezoelectric charge coefficient (d_{33}), dielectric constant (K^T_3) and relative density for the BM, DM and WM samples sintered at the 1120 °C for 2 h

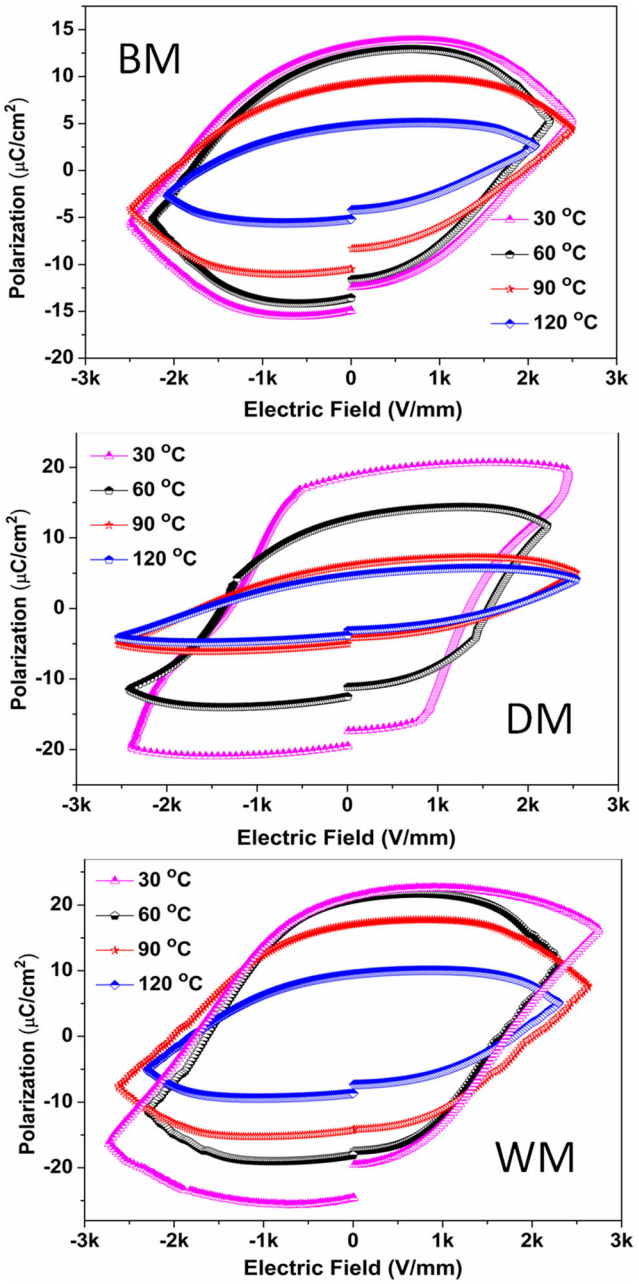

Fig. 6 Temperature-dependent ferroelectric loops of the BM, DM and WM sample sintered at 1120 °C for 2 h

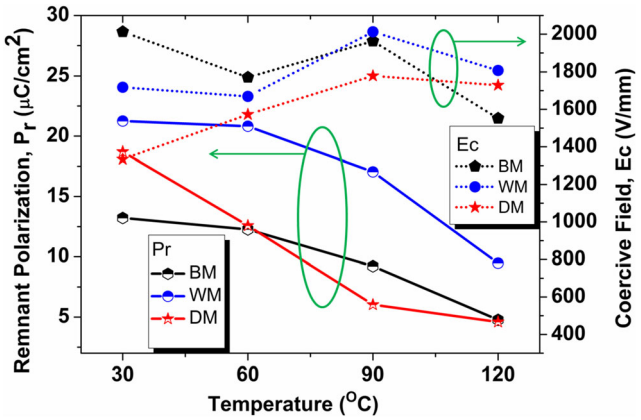

Fig. 7 Plot of remnant polarisation (P_r) and coercive field (E_c) values of the BM, DM and WM samples at different temperatures

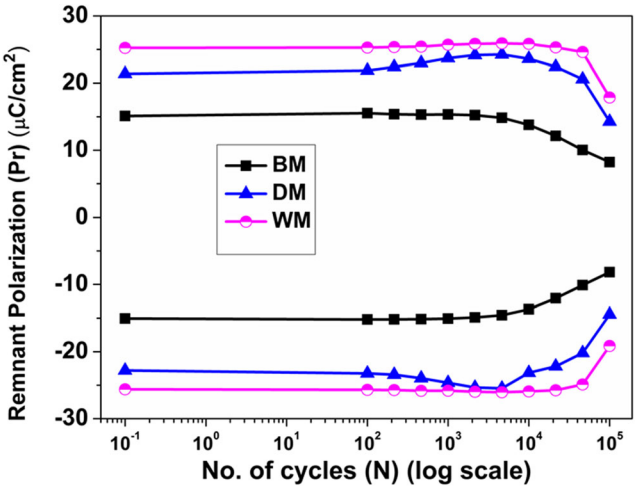

Fig. 9 Electrical fatigue of the BM, DM and WM samples under bipolar electrical switching cycle

270 nm for the DM and WM samples, respectively, as calculated using the Quantimet software. The FESEM micrographs are in good agreement with the particle size distribution.

Figure 3 shows the X-ray diffraction pattern of the sintered samples. No trace of any secondary phase was detected after sintering. The XRD patterns indicate an orthorhombic symmetry predominantly in the BM samples, which is retained even after 10 h of dry milling in DM ceramic, as evident from the splitting of the (002) and (200) characteristic peaks at $2\theta \sim 45°$ [40]. However, the WM sample depicts different crystal structure. The Rietveld refinement results are shown in Table 1, and R_{wp} and goodness of fit (GOF) have been used as parameters indicating the quality of fitting. The Rietveld refinement revealed the presence of orthorhombic (e.g. *Amm2*) phase in BM and DM samples. However, the XRD profile of WM sample could only be fitted with a combination of monoclinic (e.g. *Pm*) and orthorhombic (e.g. *Amm2*) structures. Since NKN-based compositions show the presence of orthorhombic-tetragonal polymorphic phase boundary, the refinement was tried with a combination of orthorhombic (*Amm2*) and tetragonal (*P4mm*) too, but it yielded inconsistent results. Comparing the X-ray diffraction profile and structural refinement data, it can be stated that due to the presence of solvent, less powder covers the ball surface and the entire energy is transferred to a lesser number of particles [34]. Hence, more impact energy is experienced by the particles, leading to the finer particles and distortion in the lattice, which causes the structural differences observed here.

The FESEM micrographs of the sintered samples revealing the surface morphology are shown in Fig. 4 which indicates a denser microstructure in the DM and WM samples as compared to the BM sample due to reduced particle size of the initial powder. The grain size of the BM sample is in the range of 3.97 μm. WM samples demonstrate the bimodal structure consisting of bigger amalgamated grains having indistinct interfaces with interspersed smaller vivid grains of an average size of 2.93 μm. Considering the fine particle size of the HEBM samples, the microstructures revealed by FESEM are surprising. It was expected that the fine particles will yield small grains on sintering as compared to CBM. However, the results obtained are contrary. Similar results were obtained by Kong et al. [41] in the PZT-based system. Perhaps, the efficient packing density of fine powder particles and high sintering temperature eased the amalgamation of particles, leading to bigger grains because the finer particles require lower sintering temperature for densification due to their higher reactivity.

The piezoelectric and dielectric properties and density are influenced drastically by HEBM as shown in Fig. 5.

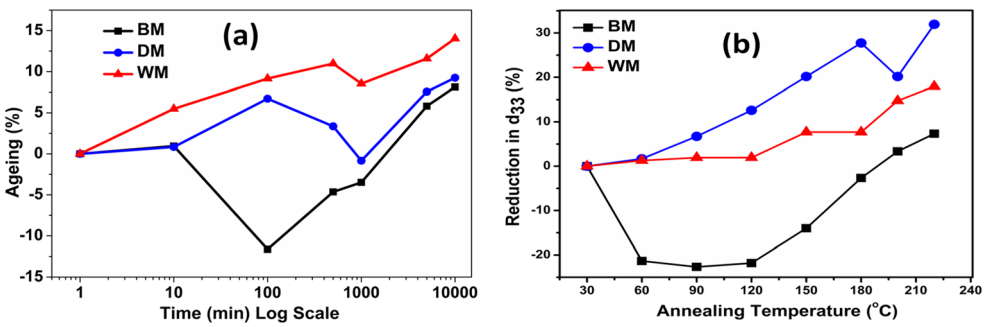

Fig. 8 **a** Ageing and **b** thermal stability of the piezoelectric charge coefficient (d_{33}) of the BM, DM and WM ceramic samples sintered at 1120 °C for 2 h

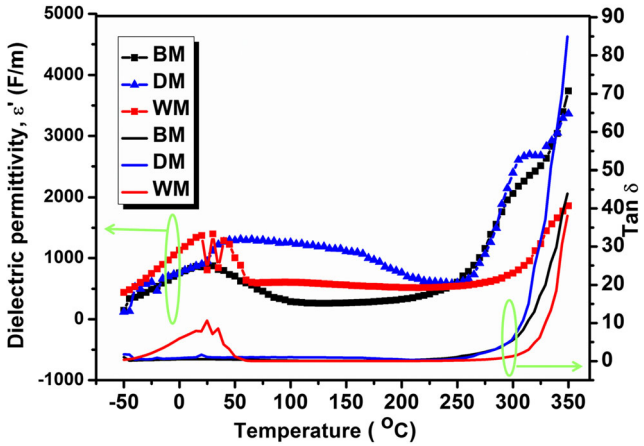

Fig. 10 Temperature dependence of dielectric constant and dielectric loss for the BM, DM and WM samples sintered at the 1120 °C for 2 h

The HEBM samples display improved properties as compared to the BM samples. In WM sample, the dielectric constant escalates to 610 from 440 in the BM sample. WM ceramic has the highest d_{33} value of 166 pCN^{-1} which can be attributed to the denser microstructure and smaller powder particle size. The monoclinic phase (*Pm*) present also plays a role in increasing piezoelectric property by easing the alignment of dipoles during the poling process due to polarisation rotation [42]. It is also proposed that perhaps, the small crystallite size and distortion caused due to HEBM enhanced the spontaneous polarisation (P_s) by influencing the interaction between B site and oxygen ion present in the perovskite lattice.

The ferroelectric loops of the samples under study at different temperatures are shown in Fig. 6. The remnant polarisation (P_r) value for the BM sample is 13.2 μC cm^{-2} at room temperature (30 °C), which increases gradually, attaining the value of 18.7 μC cm^{-2} and 21.3 μC cm^{-2} for the DM and WM samples, respectively. The BM sample exhibited the highest coercive field (E_c) (2.01 kV mm^{-1}) value as shown in Fig. 7. The ferroelectric loop of the BM sample displays a leaky capacitor behaviour which indicates the presence of a higher number of charge carriers. These results show the influence of two predominant factors: firstly, the grain size effect. The space charge, due to the presence of charge carriers, gets accumulated at the grain boundaries. Smaller grains mean more grain boundaries which are leading to the accumulation of more space charge at the grain boundaries. Second is the lower spontaneous polarisation of the perovskite lattice in the BM sample, which manifest itself in the form of lower d_{33} and P_r [36]. The other factors may be the presence of some internal stresses and the lesser number of ferroelectric domains in the BM sample which is apparent from the d_{33} values also. Temperature-dependent ferroelectric loops show stable properties in the WM sample up to 90 °C. In rest of the samples, the decay of P_r is faster. The decrease in the P_r with temperature can be attributed to the higher thermal fluctuations which reduces the ferroelectric interaction between the dipoles [43]. This substantiates our proposition that the stronger ferroelectric character in the WM sample is due to the enhanced interaction between B site cation and oxygen anion.

Figure 8a, b shows a variation of piezoelectric charge coefficient (d_{33}) for the poled BM, DM and WM ceramics while ageing and thermal annealing. It can be seen that the ageing and thermal annealing behaviour shows a similar pattern. The fluctuation of property under thermal duress and ageing is very small in the WM samples which indicates its stable piezoelectric behaviour. The slight increase in piezoelectric properties on ageing and thermal annealing is attributed to the stress relieving, which results in the favourable alignment of dipoles in polarisation direction. The DM samples exhibit the highest decline rate during thermal annealing which has been observed during the temperature-dependent ferroelectric studies too.

The fatigue under bipolar electrical loading is shown in Fig. 9. During the fatigue cycle, there is a redistribution of space charges and oxygen vacancies leading to the pinning of domain walls and, thus, reducing the P_r. The decrease of P_r is very fast in the BM sample which indicates stronger pinning in the sample due to a higher number of charge carriers and slowest in the WM sample which is due to the less charge carriers and stable ferroelectric polarisation state. The thermal annealing and fatigue results corroborate the findings of the ferroelectric study.

The influence of temperature on the dielectric permittivity (ε') and loss factor (tan δ) of the samples under study is shown in Fig. 10. The first dielectric anomaly in the BM and DM samples is observed at ~25 °C which corresponds to orthorhombic-to-tetragonal phase transition. The WM sample, however, exhibits multiple peaks at this temperature which are perhaps due to monoclinic to tetragonal, monoclinic to orthorhombic and orthorhombic to tetragonal phase transformations happening simultaneously. As the difference between orthorhombic space group (*Amm2*) and monoclinic (*Pm*) is very small, the possibility of these phase transformations cannot be ruled out [44, 45]. To know the exact nature of these transformations, a detailed study is required to be done. The second dielectric anomaly, indicating the tetragonal to cubic phase transformation (T_C), occurs at around 300 °C in the BM and DM samples. The second anomaly shifts to ~320 °C for the WM sample which again confirms the stable ferroelectric polarisation state in WM ceramic, thus necessitating higher energy to perturb it. Below the tetragonal to cubic phase transition temperature, almost all the samples possess good thermal stability beyond which the losses increase with an increase in temperature.

Conclusion

The HEBM influences the particle size drastically, which improves the piezoelectric and dielectric properties of the samples due to better density, as seen in the microstructural studies, and/or by inducing the structural changes in the lattice. The wet HEBM is found to be suitable for enhancing the properties due to higher impact energy experienced by the particles. The HEBM also incorporates a stable behaviour in NKLNT lead-free piezoceramics. The wet HEBM leads to higher piezoelectric and ferroelectric properties, with better thermal and fatigue resistance, due to the higher spontaneous polarisation of the perovskite lattice and more number of ferroelectric dipoles.

Acknowledgements The authors express their sincere gratitude to the Director of the Armament Research and Development Establishment for providing the necessary support to carry out the research work.

Compliance with ethical standards

Conflict of interest The authors declare that they have no conflicts of interest.

References

1. Haertling, G.H.: J. Am. Ceram. Soc. **82**, 797–818 (1999). https://doi.org/10.1111/j.1151-2916.1999.tb01840.x
2. Saito, Y., Takao, H., Tani, T., Nonoyama, T., Takatori, K., Homma, T., Nagaya, T., Nakamura, M.: Nature. **432**, 84–87 (2004). https://doi.org/10.1038/nature03028
3. Wang, X., Wu, J., Xiao, D., Cheng, X., Zheng, T., Lou, X., Zhang, B., Zhu, J.: ACS Appl. Mater. Interfaces. **6**, 6177–6180 (2014). https://doi.org/10.1021/am500819v
4. Zhang, B., Wu, J., Cheng, X., Wang, X., Xiao, D., Zhu, J., Wang, X., Lou, X.: ACS Appl. Mater. Interfaces. **5**, 7718–7725 (2013). https://doi.org/10.1021/am402548x
5. Guo, Y., Kakimoto, K., Ohsato, H.: Mater. Lett. **59**, 241–244 (2005). https://doi.org/10.1016/j.matlet.2004.07.057
6. Wang, Y., Damjanovic, D., Klein, N., Hollenstein, E., Setter, N.: J. Am. Ceram. Soc. **90**, 3485–3489 (2007). https://doi.org/10.1111/j.1551-2916.2007.01962.x
7. Shen, Z.Y., Xu, Y., Li, J.F.: Ceram. Int. **38S**, S331–S334 (2012). https://doi.org/10.1016/j.ceramint.2011.04.113
8. Zhou, J.J., Li, J.F., Zhang, X.W.: J. Mater. Sci. **47**, 1767–1773 (2012). https://doi.org/10.1007/s10853-011-5957-y
9. Shen, Z.Y., Wang, K., Li, J.F.: Appl. Phys. A. **97**, 911–917 (2009). https://doi.org/10.1007/s00339-009-5358-0
10. Skidmore, T.A., Comyn, T.P., Milne, S.J.: Appl. Phys. Lett. **94**, 222902 (2009). https://doi.org/10.1063/1.3153157
11. Kim, M.S., Lee, D.S., Park, E.C., Jeong, S.J., Song, J.S.: J. Eur. Ceram. Soc. **27**, 4121–4124 (2007). https://doi.org/10.1016/j.jeurceramsoc.2007.02.194
12. Bai, L., Zhu, K., Qiu, J., Ji, H., Su, L.: Particuology. **8**, 477–481 (2010). https://doi.org/10.1016/j.partic.2010.05.007
13. Fang, J., Wang, X., Li, L.: J. Am. Ceram. Soc. **94**, 1654–1656 (2011). https://doi.org/10.1111/j.1551-2916.2011.04534.x
14. Gu, Q., Zhu, K., Liu, J., Wang, J., Qiu, J., Cao, Y., Liu, P., Yao, L.: J. Nanosci. Nanotechnol. **15**, 4934–4940 (2015). https://doi.org/10.1166/jnn.2015.9848
15. Lee, J.S., Choi, M.S., Hung, N.V., Kim, Y.S., Kim, I.W., Park, E.C., Jeong, S.J., Song, J.S.: Ceram. Int. **33**, 1283–1286 (2007). https://doi.org/10.1016/j.ceramint.2006.04.017
16. Praveenkumar, B., Kumar, H.H., Kharat, D.K., Murty, B.S.: Mater. Chem. Phys. **112**, 31–34 (2008). https://doi.org/10.1016/j.matchemphys.2008.04.009
17. Praveenkumar, B., Sreenivasalu, G., Kumar, H.H., Kharat, D.K., Balasubramanian, M., Murty, B.S.: Mater. Chem. Phys. **117**, 338–342 (2009). https://doi.org/10.1016/j.matchemphys.2009.06.032
18. Kong, L.B., Ma, J., Zhu, W., Tan, O.K.: Mater. Res. Bull. **37**, 459–465 (2002). https://doi.org/10.1016/S0025-5408(01)00823-6
19. D. Kuscer, J. Holc, M. Kosec, 90 (2007) 29–35. doi:https://doi.org/10.1111/j.1551-2916.2006.01332.x
20. Liu, X.J., Huang, Z.Y., Pu, X.P., Sun, X.W., Huang, L.P.: J. Am. Ceram. Soc. **88**, 1323–1326 (2005). https://doi.org/10.1111/j.1551-2916.2005.00227.x
21. Dash, S.K., Kant, S., Dalai, B., Swain, M.D., Swain, B.B.: Indian. J. Phys. **88**, 129–135 (2014). https://doi.org/10.1007/s12648-013-0395-0
22. Kaczmarek, W.A.: J. Mater. Sci. **31**, 5271–5279 (1996). https://doi.org/10.1007/BF00355934
23. Kong, L.B., Zhu, J.W., Tan, O.K.: Ferroelectrics. **230**, 281–286 (1999). https://doi.org/10.1080/00150199908214932
24. Hao, J., Zhai, J., Li, Y.: Jpn. J. Appl. Phys. **50**, 110207 (2011). https://doi.org/10.1143/JJAP.50.110207
25. Singh, K.C., Jiten, C.: Mater. Lett. **65**, 85–88 (2011). https://doi.org/10.1016/j.matlet.2010.09.057
26. Jiten, C., Rawat, M., Bhattacharya, A., Singh, C.: Mater. Res. Bull. **90**, 162–169 (2017). https://doi.org/10.1016/j.materresbull.2017.02.031
27. Liu, S., Zhang, L., An, L., Fei, W., Heinrich, H.: J. Am. Ceram. Soc. **88**, 2559–2563 (2005). https://doi.org/10.1111/j.1551-2916.2005.00457.x
28. Chen, X.M., Gong, X.X., Li, T.N., He, Y., Liu, P.: J. Alloys Compd. **507**, 535–541 (2010). https://doi.org/10.1016/j.jallcom.2010.08.012
29. Han, H.S., Heo, D.J., Dinh, T.H., Lee, C.H., Kang, J.K., Ahn, C.W., Tran, V.D.N., Lee, J.S.: Ceram. Int. (2017). https://doi.org/10.1016/j.ceramint.2017.03.038
30. Van, N.D.: Adv. Mater. Sci. Eng. 230216 (2013). https://doi.org/10.1155/2013/230216
31. Van, N.D.: Sci. World J. 203047 (2014). https://doi.org/10.1155/2014/203047
32. Liu, L., Wu, M., Huang, Y., Fang, L., Fan, H., Dammak, H., Thi, M.P.: Mater. Res. Bull. **46**, 1467–1472 (2011). https://doi.org/10.1016/j.materresbull.2011.05.001
33. Zuo, R., Rodel, J., Chen, R., Li, L.: J. Am. Ceram. Soc. **89**, 2010–2015 (2006). https://doi.org/10.1111/j.1551-2916.2006.00991.x
34. BenAbdeslam, H.E.B., Ginebra, M.P., Vert, M., Boudeville, P.: Acta Biomater. **4**, 378–386 (2008). https://doi.org/10.1016/j.actbio.2007.07.003
35. Byeon, S., Yoo, J.: J. Electroceram. **33**, 202–207 (2014). https://doi.org/10.1007/s10832-014-9948-7
36. Rawal, B., Wathore, N.N., Praveenkumar, B., Panda, H.S.: J. Mater. Sci. Mater. Electron. **28**, 16426–16432 (2017). https://doi.org/10.1007/s10854-017-7553-7
37. Zhou, J., Li, J., Cheng, L., Wang, K., Zhang, X., Wang, Q.: J. Eur. Ceram. Soc. **32**, 3575–3582 (2012). https://doi.org/10.1016/j.jeurceramsoc.2012.05.019
38. Paula, A.J., Parra, R., Zaghete, M.A., Varela, J.A.: Solid State Commun. **149**, 1587–1590 (2009). https://doi.org/10.1016/j.ssc.2009.06.041

39. Yashima, M., Hoshina, T., Ishimura, D., Kobayashi, S., Nakamura, W., Tsurumi, T., Wada, S.: J. Appl. Phys. **98**, 014313 (2005). https://doi.org/10.1063/1.1935132
40. Skidmore, T.A., Milne, S.J.: J. Mater. Res. **22**, 2265–2272 (2007). https://doi.org/10.1557/JMR.2007.0281
41. Kong, L.B., Ma, J., Zhu, W., Tan, O.K.: Mater. Lett. **46**, 274–280 (2000). https://doi.org/10.1016/S0167-577X(00)00185-3
42. Fu, H., Cohen, R.E.: Nature. **403**, 281–283 (2000). https://doi.org/10.1038/35002022
43. Wongdamnern, N., Triamnak, N., Ngamjarurojana, A., Laosiritaworn, Y., Ananta, S., Yimnirun, R.: Ceram. Int. **34**, 731–734 (2008). https://doi.org/10.1016/j.ceramint.2007.09.048
44. Baker, D.W., Thomas, P.A., Zhang, N., Glazer, A.M.: Appl. Phys. Lett. **95**, 091903 (2009). https://doi.org/10.1063/1.3212861
45. Tellier, J., Malic, B., Dkhil, B., Jenko, D., Cilensek, J., Kosec, M.: Solid State Sci. **11**, 320–324 (2009). https://doi.org/10.1016/j.solidstatesciences.2008.07.011